Experimental determination of fracture toughness of epoxy toughened with nano-block copolymers

Adam T. Lachlan[1]

University of New South Wales at the Australian Defence Force Academy

A lack of resistance to crack growth and initiation limits the application of epoxy in fields requiring high fracture toughness. Means to improve the fracture toughness of epoxy are commonly achieved through the addition of a secondary phase. The study of increasing levels of Nanostrength® M52N nano-block copolymers with a bisphenol A epoxy resin has been investigated due to low agglomeration of the nanophase, and retention of mechanical and thermal properties signature to epoxy. Mode I fracture toughness has been determined using double cantilever beam testing. A modified simple beam theory for brittle, linear elastic behaviour, has accounted for bond line properties and non-symmetrical crack propagation of the adherend. Experimental investigation has shown improvements of stress intensity factor for Mode I failure, K_{Ic}, of 173% for 10% volume fracture nanophase.

Contents

Nomenclature

a	=	crack length [mm]
a_0	=	initial crack length [mm]
a_{SBT}	=	apparent crack length [mm]
B	=	width of DCB specimens [mm]
C	=	compliance, δ/P [mm/N]
DCB	=	double cantilever beam
e	=	adherend thickness [mm]

[1] SBLT, School of Engineering & Information Technology. ZEIT4501

E_a = Young's modulus of adherend [Pa]
E_s = Young's modulus of aluminium substrate [Pa]
G = strain energy release rate [J/m^2]
G_a = adhesive fracture energy [J/m^2]
G_{Ic} = critical strain energy release rate [J/m^2]
h = substrate thickness [mm]
K = Stress intensity factor [Pa√m]
K_{Ic} = Critical stress intensity factor [Pa√m]
P = applied load [N]
δ = load point displacement [mm]

I. Introduction

A. Background

The use of epoxy in a wide range of industries can be attributed to many outstanding mechanical and thermal properties such as, high modulus and chemical resistance, low shrinkage upon curing, electrical insulation and, the ability to be processed under a variety of conditions (Barsotti 2008; Hsieh et al. 2010; Khurana et al. 2003). Epoxy is a thermosetting material, which inherently is brittle due to being highly amorphous and cross-linked (Kinloch 2003; Morozov 2013; Yang 1998). In structural environments, epoxy is primarily used as the matrix constituent of composite materials. The adhesive qualities of epoxy are highly attractive whereby; existing practices of adhering structures by mechanical means can be eliminated (Jumel et al. 2013). Mechanical means induce stress concentrations for crack growth, which can be eliminated through the use of adhesively bonded materials. However, the *fracture toughness*, the resistance to crack growth and initiation, limits the application of epoxy for structural purposes (Bagheri et al. 2009; Hossein et al. 2013). As a result, extensive studies to improve the toughness of epoxy have been undertaken (Bagheri et al. 2009; Yahyaie et al. 2013; Yang 1998; Zhao & Hoa 2007). Improvement of fracture toughness of epoxy can be achieved through the incorporation of dispersed toughener phase(s) in the epoxy matrix, by means of rubbers, thermoplastics, silica, carbon fibres; being of micro and nanoscale (Bagheri et al. 2009; Yang 1998).

The selection of phase additive can not only improve fracture toughness but in addition, deteriorate mechanical and thermal properties. A rubber phase increases the viscosity of epoxy, and hence reduces matrix modulus (Hseih et al. 2010; Kinloch et al. 2007). Accordingly, a means to improve fracture toughness without sacrificing modulus or viscosity; and other mechanical and thermal properties, is overcome through a nanophase (Barsotti 2008; Hsieh et al. 2010; Kinloch et al. 2007; Wetzel et al. 2006; Zamanian et al. 2012; Zhao & Hoa 2007). The improvement to epoxy modulus, yield strength and fracture toughness is greatly enhanced with smaller, nano-size fillers than larger, micro-size fillers (Mostovoy & Ripling 1966; Zamanian et al. 2012).

For this study, Nanostrength® M52N nano-block copolymers are used as a secondary phase additive. Barsotti (2008) has developed a new method to synthesise a triblock copolymer consisting of polymethylmethacrylate-b-polybutylacrylate-b-polymethylmethacrylate (PMMA) that, self-assembles in the nanoscale by controlled radical polymerization and anionic polymerization. This eliminates agglomeration (lumping) issues of more frequently used nano clay, nano silica and carbon nano tubes (Kinloch et al. 2007; Kishi et al. 2011). Figure 1 confirms by transmission electron microscopy (TEM) imagery of 10% triblock copolymers in DGEBA resin with no evidence of agglomeration. Block copolymers are known for having nano-phase structures themselves (Bates & Fredrickson 1999; Kishi et al. 2011). The chemical structure of the copolymers and a schematic illustration of the nano-phase structure are shown in Fig. 2. Nano structure is formed from the phase separation of the middle and side blocks, driven by chemical incompatibilities of the blocks that make up the copolymer chain (Bates & Fredrickson 1999).

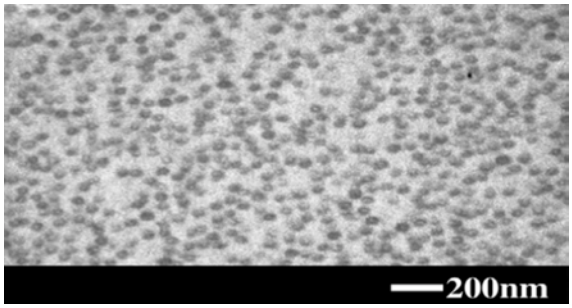

Figure 1. TEM of 10% triblock copolymers in DGEBA resin (Kishi et al. 2011)

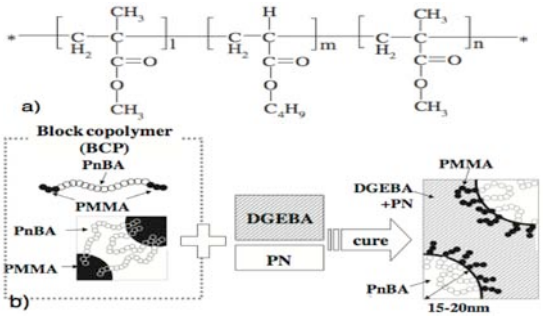

Figure 2. a) Chemical structure of PMMA. b) Nanophase structure schematic (Kishi et al. 2011)

Barsotti (2008) has reported upon the improved fracture toughness of nano-block copolymers for bulk epoxy under ASTM D 5045, single edge notched bending (SENB) testing, with results showing a 10% volume fraction of nano-blocks improves neat epoxy Mode I stress intensity factor, K_{Ic}, by 207% from 0.88 MPa.m$^{0.5}$ to 1.82 MPa.m$^{0.5}$. In addition, Barsotti (2008) comments that material modulus and glass transition temperature are not adversely affected due to the non-reactive backbone of the block copolymers. However, and converse to Barsotti, the fracture toughness of thin layer-epoxy has been examined based upon the background application of epoxy resin in adhesive environments than as bulk specimens under ASTM D 5045 for plane strain conditions.

B. Aim

To investigate and determine the Mode I fracture toughness due to the addition of nano-block copolymers at varying levels for thin film adhesive epoxy.

C. Methodology

The failure of a material may result from one of three different modes, or a mixture thereof. Mode I failure is described as tensile, or opening mode (Broberg 1999), characterized by tensile stress normal to the plane of the crack. Mode II is in-plane shear, and Mode III is out-of-plane shear. Failure is typically Mode I, where as Modes II and III, is uncommon and occurs in a combined fashion (Shukla 2005). Figure 3 illustrates the three fracture modes.

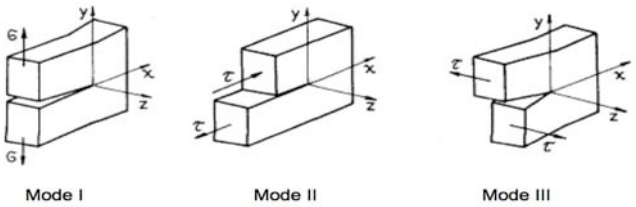

Figure 3. Fracture modes (Le Baut 2005)

In a cracked body, the load that causes a stationary crack to propagate rapidly is associated with the fracture toughness (for initiation) and, the load that causes a running crack to stop is associated with an arrest toughness (Mostovoy & Ripling 1966). Therefore, fracture toughness is observed as a material property that measures resistant to extension of a pre-existing crack. Whether it is evaluated for initiation or arrest, fracture toughness can be defined in terms either strain energy release rate, G, or stress intensity factor, K. The stress intensity approach evaluates the zone around the crack tip where as strain energy release rate addresses an energy approach to crack initiation and growth. The units of K are MPa.m$^{0.5}$ and G, J/m^2. Mode I testing of strain energy release rate is commonly determined using the double cantilever beam (DCB) method as the test addresses brittle, linear elastic behaviour (Brunner et al. 2001; Lamut et al. 2008). Linear elastic fracture mechanics (LEFM) assumes a linear elastic body contains a sharp crack and then, continues to describe the energy change that occurs within that body as the crack grows (Lamut et al. 2008; Shukla 2005). There are two basic configurations for the DCB specimens, the constant width and the Tapered DCB (TDCB). The width of the tapered specimen is designed such that crack length, a, divided by specimen width, B, is constant (Mostovoy & Ripling 1966; Sela & Ishai 1989). Consequently, the strain energy release rate derived from the analysis of a TDCB specimen is independent of crack length, and the crack grows under constant load. This means monitoring of the crack length during the test is eliminated (Mostovoy & Ripling 1966). However, the fabrication of the tapered composite specimen is much more complicated than constant width (Sela & Ishai 1989). Constant width DCB is simple and inexpensive to fabricate (Abou-Hamda et al. 1998) and hence, has been used as the configuration for Mode I determination. A schematic representation of the DCB test is shown in Fig. 4.

Adopting a standard test method allows the user to have confidence in the procedure as it has been evaluated appropriate. By using a standard, the results can be replicated or compared for different materials, specimen sizes, load rates etc. within the standard's constraints. This methodology has been applied in conjunction with published peer-reviewed articles to form a *best fit the practice* for this thesis. The American Society for Testing and Materials (ASTM) determines Mode I fracture toughness of Fibre-Reinforced Polymer (FRP) Matrix Composites (ASTM International 2007) and British Standard (BS) 7991:2001 determines Mode I adhesive fracture energy G_{Ic} of structure adhesives for DCB and TDCB specimens (British Standard 2001). Although strictly applicable to composites of

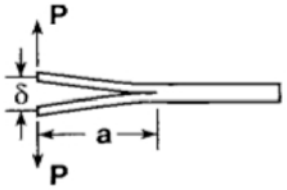

Figure 4. Double Cantilever Beam Schematic (ASTM International 2007)

unidirectional carbon fibre and glass fibre tape laminates, ASTM D 5528 is highly applicable to DCB manufacturing and testing of metallic adhered specimens (ASTM International 2007). A point of concern when loading FRPs is delamination and it's effect on G_{Ic}. Delamination between the layers of composites would influence the value of fracture toughness of the adherend. For composite-layered materials, the crack does not always follow the theoretically preferred path of fracture; the crack front may wander and follow fibre-matrix interfaces due to a variation in G across the width of the test specimen (Pagano & Schoppener 2000). Similarly, and of particular interest, is BS 7991:2001, which is well suited for the determination of fracture resistance of structural adhesive joints under Mode I tensile loading conditions (British Standard 2001). This test method is well suited for testing adhesive bond toughness of relatively thin sheets however, may also be used with metallic substrates which possessive relatively high yield stress (British Standard 2001). The use of both ASTM D 5528 and BS 7991:2001 is based upon the near-interchangeable instructions, to each other, for determining G_{Ic} of an adhesive under Mode I testing via DCB. Areas not covered in the methodology of one standard are often covered by the other standard.

II. Experimental

A. Procedure

Double cantilever beam methodology involves the separation of two adhered substrates to invoke crack propagation within the adherend. All tests were conducted under controlled displacement at a crosshead speed of 0.1 mm/min using a Shimadzu universal testing machine. Displacement controlled testing was used to initiate stable crack growth propagation. The specimen is attached to the machine grips by the hinges, shown in Fig. 5. The specimen hinges were loaded to produce crack growth totaling 120 mm in length. Applied force, P, was measured with a 50 kN load cell. Opening displacement, δ, was measured with a 50 mm laser extensometer, LE 05. At least five specimens per volume fraction ratio of nano-blocks were manufactured and tested. This was for volume fraction ratios of 0%, 2.5%, 5.0% and 10.0% nano-block copolymer-resin.

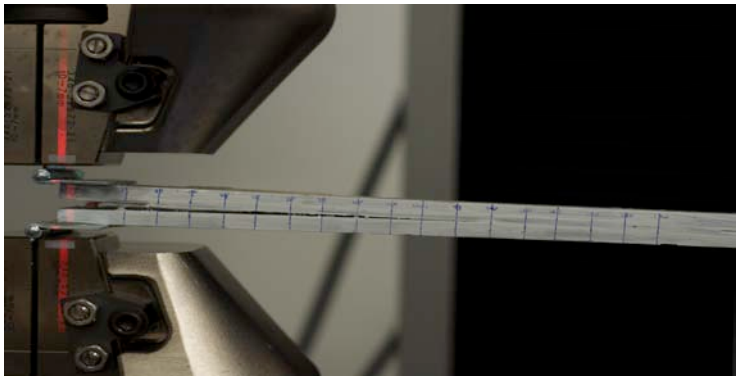

Figure 5. Specimen in Shimadzu universal testing machine

B. Preparation of Specimens

The preparation of the specimens was done in accordance with a risk assessment produced, seen in Appendix A. The budget associated with this project is included in Appendix B.

The adherends used were aluminium alloy 6060 with a Young's modulus, E = 69.5 GPa (Dalsteel Metals Pty Limited 2014). The substrate thickness, h, of 5.8 mm was chosen such that no plastic strain and asymmetric loading was observed in the aluminium during the tests. The substrates were 25 mm in width, B, and 210 mm in length. The surfaces of the aluminium were prepared to provide confidence that cohesive, rather than adhesive, failure was to be the principle mode of failure. Firstly, adherend surfaces were wiped free of grease, oil and dust with a clean cloth and acetone. The surface was then grit-blasted using a Burwell 'Tornado' bead blaster at an operating pressure of 340 kPa with silica beads until the surface appeared uniform. Following, the substrates were washed in an acetone bath for 30 minutes, and then rinsed with distilled water and dried with a hair-dryer. Surfaces were bonded with a five-to-one part West System® 105 bisphenol A based epoxy resin, and West System® 206 slow hardener. Nano-blocks were combined with epoxy resin in a beaker at 40°C on a magnetic-thermal stirrer at a low rate for one hour. Nanostrength® was added moderately to ensure lumping did not occur. The addition of hardener was done with room temperature cooled resin to improve working time. Resin and hardener was hand mixed using a tongue depressor. As a result, porosities and void in the adhesive resulted, seen in Fig. 6.

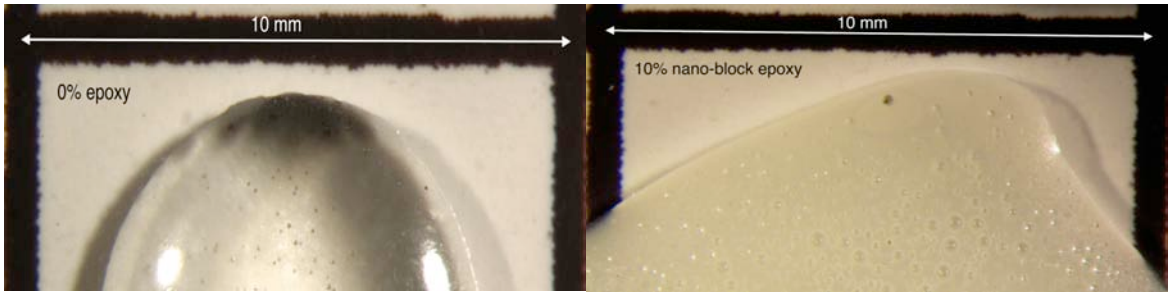

Figure 6. Porosities and voids within epoxy *Left: 0% specimen, Right: 10% specimen*

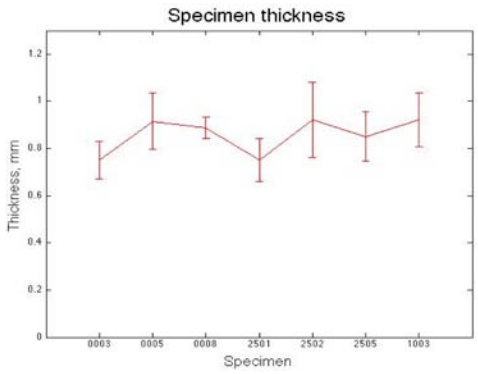

Figure 7. Thickness variation amongst specimens

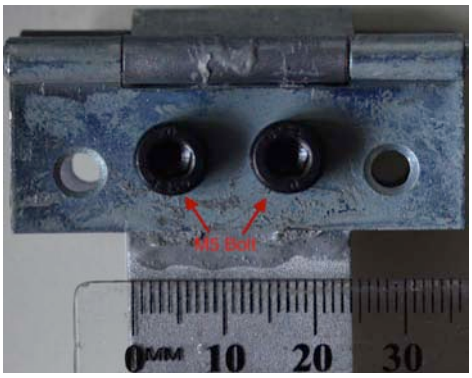

Figure 8. Bolted hinge

External pressure was applied to the substrates to improve epoxy-aluminium bond strength and minimise porosities within the adherend however, it was noted that excessive amounts of epoxy was excreted between the substrates and non-uniform bond line thickness' formed. In order to overcome this, the specimen had a shim of thickness of 0.218 mm added to each end. Using *ImageJ64*, cured specimens were examined to determine the mean bond thickness along the specimen length; and hence a bond line thickness for further calculations. Shown in Fig. 7 is a plot of the mean thickness with corresponding error bar of one standard deviation. The mean of the adherend thickness for seven samples is 0.830 mm with a standard deviation of 0.126 mm. The variability of thickness amongst the specimens is not significant as the error bars all overlap each other; there is confidence to say the thickness of any specimen is between 0.704 mm to 0.956 mm.

Polytetrafluroethylene (PTFE), *Teflon*, tape was placed at one end of the specimen, mid-plane in order to form a delamination site for a natural crack to be induced by a scraper blade (when tapped). Such forced crack propagation by tapping was arrested with a clamping collar to an initial crack length, a_0, of 50 mm. The PTFE end of the specimen was cut with a *cold saw* in order to remove the shim from the specimen, and allow access to the delamination site. A belt sander removed excess epoxy excreted from curing. This surface was then coated with whiteout, and incrementally marked at 10 mm, to aid visual observation of the crack front formation during testing. Hinges were bonded at the crack-end of the specimen to provide the necessary means to pull the two aluminium substrates apart; and hence grow the crack. Zenith 50 mm zinc plated fixed pin butt hinges were bonded with Epirez 8242, high strength structural-adhesive (Epirez 2011). The bonding surface of the hinge and aluminium were prepared in the same manner as the substrate-adherend surface. The hinges were clamped with bulldog clips during curing.

An extension was conducted to bonding of the hinges; rather the hinges were bolted. Specimens 0009, 0011, 0012, 0013, 1003, 1004, and 1005 had the hinges bolted to the aluminium substrate with two M5 bolts. Adhesive failure occurred between the hinge-substrate interface, and hence, a means to secure the hinges to the aluminium was achieved with bolts. Figure 8 illustrates a bolted hinge specimen.

III. Comparison of Analysis Methods

The analysis of adhesive fracture toughness is outlined by Blackman et al. (1991) where, under LEFM the load-displacement traces result in four, theoretically identical results. Blackman et al. formulates fracture toughness as G_a, adhesive fracture toughness. This is considered the same as G_{Ic}. Figure 9 illustrates a typical load versus displacement trace by Blackman et al., for the DCB specimen using a two-part cold-cure epoxy-paste adhesive bonding poly(etherether ketone) unidirectional carbon-fibre composites. The specimen is loaded until approximately 300 N where the crack initiates and begins to grow.

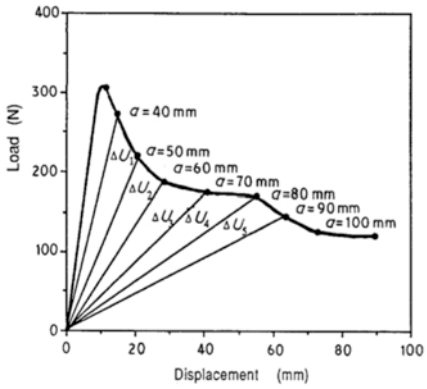

Figure 9. Typical load versus displacement curve (Blackman et al. 1991)

The first method, defines G_a where elastic behaviour exists using an area method:

$$G_a = \frac{\Delta U}{B\Delta a} \tag{1}$$

where B is the width of the DCB specimen, ΔU is the area under the load-displacement trace and Δa is the increase in crack length from a_1 to a_2. The second method, the *compliance method*, determines the value of adhesive fracture energy, G_a, for an LEFM test by:

$$G_a = \frac{P^2}{2B}\left(\frac{dC}{da}\right) \tag{2}$$

where P is the load and C is the compliance, given by $C = \delta/P$. Where δ, is the displacement corresponding to a load P. To evaluate G_a using the *compliance method*, a plot of C versus the crack length, a, may be constructed. The plot of C against a is then curve fitted using a cubic function, see Eq. (3) and differentiated, see Eq. (4). Knowing the value of the load, P, and the differential dC/da, at a given crack length, then the value of G_a as a function of the crack length may be evaluated using Eq. (2).

$$C = \frac{\delta}{P} = \frac{2a^3}{3E_sI} \tag{3}$$

$$\frac{dC}{da} = \frac{2a^2}{E_sI} \tag{4}$$

A third approach to analysing the data is based upon simple beam theory (SBT). Given $E_s >> E_a$ then the second moment of area can be approximated, $I \approx Bh^3/12$; substrate thickness is given by h, Young's modulus of the substrate is E_s and adherend Young's modulus is E_a. Hence compliance is given be the following:

$$C = \frac{8a^3}{BE_sh^3} \tag{5}$$

Differentiating Eq. (5) and substituting into Eq. (2), gives:

$$G_a = \frac{P^2a^2}{BE_sI} \tag{6}$$

The fourth method, *displacement method*, substitutes P from Eq. (3) into Eq. (6), yielding Eq. (7):

$$G_a = \frac{3P\delta}{2Ba} \tag{7}$$

As stated by Blackman et al. (1991), the four methods outlined are theoretically identical and have been confirmed using load versus displacement plots for specimens of this study. However, the accuracy of methodology does give rise to sources of error (Blackman et al. 1991; Hashemi et al. 1990). Blackman et al. (1991) acknowledges work undertaken by Hashemi et al. (1990) whereby correction factors have been

incorporated for load, displacement and compliance. The effect of testing beams with relatively low shear modulus can lead to rotations and deflections occurring at the crack tip. Such effects are ignored in the simple beam analyses, which assume that the compliance at the crack root is zero, i.e. the arms act as built-in cantilever beams. In addition, slender substrate arms can often undergo large, albeit linear, displacements during testing which, when combined with end-block that tilt as the arm bends, can lead to an effective shortening of substrate arms. Overcoming these errors can be achieved through the use of metallic substrate arms, rather than through the use of polymeric fibre-composite substrates.

A further extension to adhesive fracture energy is defined by Salem et al. (2013) whereby DCB standard testing for Euler-Bernoulli beam bending theory has been refined, allowing better estimation of crack front position, as well as fine investigation of stress distribution along the bond line. Various reduction methods for adhesive fracture toughness fail to acknowledge the influence of bond line properties (Irwin & Kies 1954; Salem et al. 2013). Salem et al. (2013) observed during testing that crack propagation was effectively cohesive but near the interface, similarly as shown in Fig. 12; crack propagation is not symmetrical. Due to the thin coating of the adhesive, the flexural rigidity of the substrate increases. This effect is sufficient to be measurable and to allow determination of mechanical properties of the coating. Accordingly, Eq. (3) is modified to take into account the effect of induced asymmetry and lower, δ_1, and upper δ_2, deflections:

$$\delta_1 = \frac{Pa^3}{3E_sI}, \quad \delta_2 = \frac{Pa^3}{3E_sI_{eff}} \tag{8}$$

Due to the adhesive coating, the upper adherend flexural rigidity, E_sI_{eff}, is increased and can be evaluated using laminate theory (Nicu & Bergaud 1999):

$$E_sI_{eff} = \frac{B(E_s^2h^4 + E_a^2e^4 + E_shE_ae(4h^2 + 6he + 4e^2))}{12(E_sh + E_ae)} \tag{9}$$

Specimen opening is given by the sum of deflections, $\delta = \delta_1 + \delta_2$. Hence compliance, C, is:

$$C = \frac{\delta}{P} = \frac{a^3}{3}\left(\frac{1}{E_sI} + \frac{1}{E_sI_{eff}}\right) \tag{10}$$

As load, P, and displacement, δ, has been monitored continuously then, an apparent crack length, a_{SBT}, according to SBT is shown by Eq. (11). This value is higher than the real, geometrical crack length since the specimen compliance is higher than that determined with SBT due to the effect of adhesive layer compliance (Salem et al. 2013).

$$a_{SBT} = \sqrt[3]{\frac{3\delta}{P\left(\frac{1}{E_sI} + \frac{1}{E_sI_{eff}}\right)}} \tag{11}$$

Fracture toughness is evaluated by adjusting Eq. (6) to account for induced asymmetry:

$$G_I = \frac{P^2a_{SBT}^2}{2B}\left(\frac{1}{E_sI} + \frac{1}{E_sI_{eff}}\right) \tag{12}$$

Previous work by Salem et al. (2013) has shown that using the apparent crack length value with the SBT formula for strain energy release rate, Eq. (12) enables a self-correction of the adhesive compliance effect. The comparison of the fracture toughness determined using Eq. (8) and Eq. (14) show results that are near identical. Observing Appendix C, the adhesive fracture toughness of the two methodologies for specimens loaded by continuously loaded or load-unload scenarios both illustrate no difference in G_{Ic}; with error bars of standard error of the mean providing further confidence that the difference of the two methods in negligible.

IV. Results and Discussion

The conduct of the testing required at least five specimens of testing per volume fraction of nano-block toughened epoxy. The data acquired from testing was analysed with Salem et al. methodology, Eq. (12). The use of Salem et al. removes the requirement to monitor crack front propagation during testing, as an apparent crack

length based upon continuous load-displacement plots are the only necessary inputs. This assists in both accuracy of crack from crack front location, that otherwise would need to be visually approximated, and reduces post-testing-analysis of crack front location to corresponding load and displacement data points. Specimens evaluated using Eq. (12) improve the accuracy of adhesive fracture toughness by accounting for adhesive compliance and non-symmetrical crack growth in the adherend, that aren't accounted for in Eq. (6). Table 1 presents the values for mean fracture toughness with standard deviation and standard error of each specimen. Fracture toughness is determined from the point of maximum load, until the completion of testing. The value determined for G_I is theoretically constant, however noise and fluctuations, in what should be steady crack growth (as a result of porosities and voids within adherend), cause variation in G_I. Figure 10 presents the mean fracture toughness for a given sample volume fraction ratio. Blue bars represent fracture toughness, and error bars of standard error are red. Specimen XXYY designates XX as a volume fraction percentage and YY the specimen number of its volume fraction series i.e. specimen 2501 is a 2.5% volume fraction nano-block to resin mixture, and is the first specimen in that volume fraction series.

Table 1: Fracture toughness, G_{Ic}, of evaluated specimens

Specimen	Mean (J/m^2)	Standard Deviation (J/m^2)	Standard Error (J/m^2)
0001	5.3	2.339	0.219
0002	7.8	1.046	0.125
0003	55.5	2.102	0.152
0006	47.4	21.288	10.644
0007	10.4	3.655	1.828
0008	44.3	15.229	7.615
0009	116.7	6.620	0.278
0011	100.3	8.541	0.374
0012	121.0	10.436	0.458
0013	118.4	14.034	0.723
2501	69.6	5.967	0.394
2502	43.4	2.762	0.179
2503	18.3	5.201	0.817
2504	32.6	5.033	2.251
2505	12.3	1.382	0.109
2506	13.5	6.395	3.197
5001	44.9	9.545	0.347
5002	53.0	3.958	0.143
5003	11.9	2.756	0.179
5004	11.1	0.968	0.049
5005	63.1	6.126	0.340
5006	114.7	22.038	1.040
5007	60.2	2.601	0.081
5008	47.1	21.179	1.902
1003	622.6	55.696	1.628
1004	428.0	36.577	3.125
1005	184.5	14.604	0.326
1006	234.6	11.441	0.368
1007	217.1	8.818	0.272

A. Significance of Precrack

The validity of these specimens is misrepresented upon inspection of fracture toughness value alone. In particular, the formation of a natural crack from precracking may lead alternatively to adhesive failure between adherend and substrate rather than within the adherend; cohesive. Specimen 0007, as with specimens 2503, 2505, 2506, 5003, and 5004, have significantly lower fracture toughness values relative to their volume fraction counterparts. As illustrated in Fig. 11, the precrack location of specimen 5003 fails to be within the adherend and rather, interfacial. Compared with Fig. 12, the precrack has induced a natural crack within the adherend of specimen 1003. As crack propagation continues with testing, the crack front of specimen 1003 becomes non-symmetrical and near interfacial, yet still cohesive. This difference in natural crack formation provides reason to whether fracture toughness of the adhesively failed specimens can validly be used. Adhesive failure does not

allow use of Eq. (12), yet for non-symmetrical, effectively cohesive failure, Salem et al. (2013) methodology is applicable.

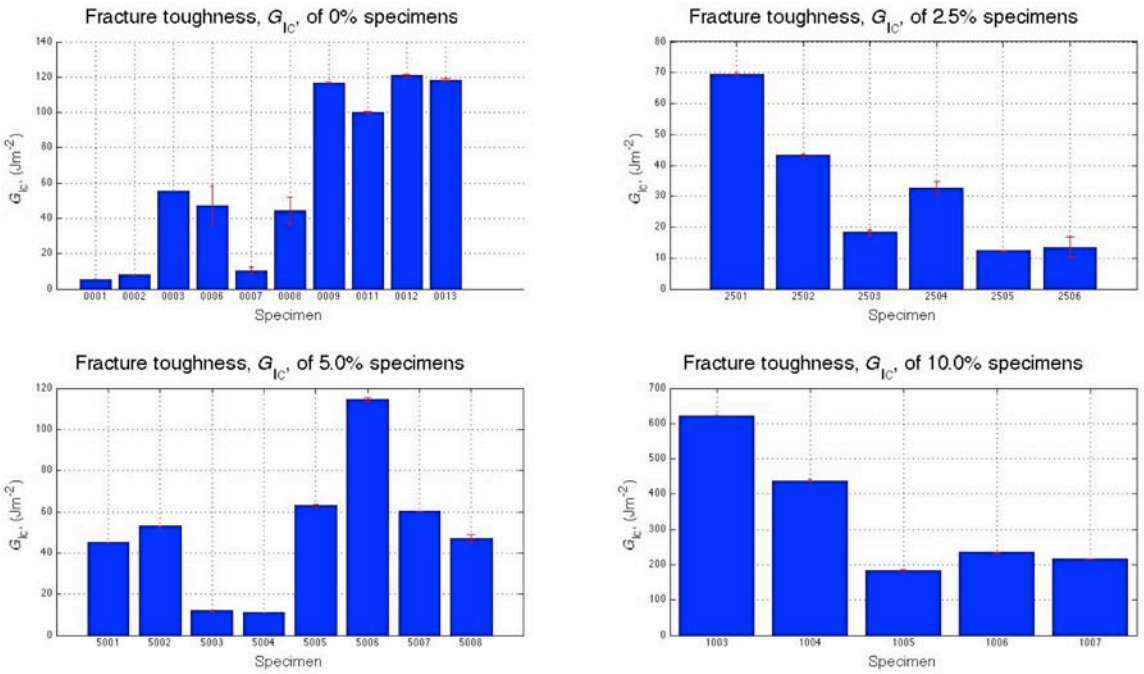

Figure 10.Strain energy release rate, G_{Ic}, of epoxy at varying nano-block copolymer volume fractions

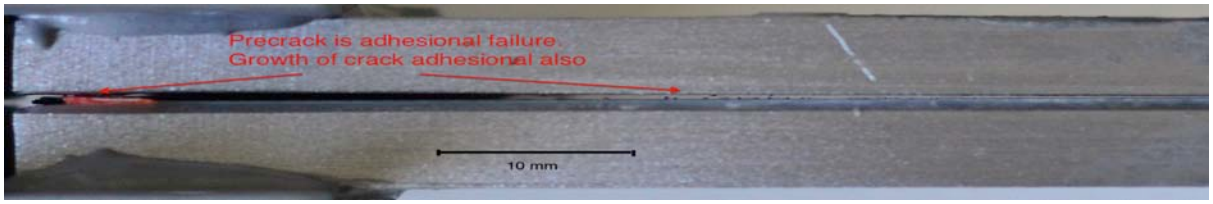

Figure 11. Adhesive failure specimen 5003

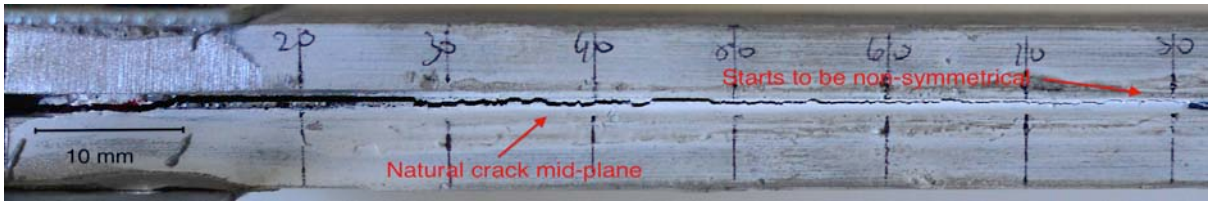

Figure 12. Cohesive failure specimen 1003

B. Critical Strain Energy Release Rate (G_{Ic})

The resulting fracture toughness for 0% nanophase specimens range from 5.3 J/m^2 to 121.0 J/m^2. Initially, the hinges of specimens 0001 and 0002 were bonded with Loctite® Super Glue Liquid Control™ however, testing resulted in failure by adhesive failure at the hinge-substrate interface. The failure of the hinge-substrate interface occurred prior to a crack propagating within the adhesive. Standard ASTM D 5528 indicates the bond adherend for the hinge may be done with superglue, or an alternate form of cyanoacrylate. The standard continues by stating that failure of the hinge-substrate interface may be improved by *a more sophisticated* cleaning process based on degreasing or chemical etching; alternatively a room temperature cure adhesive. As such, Epirez 8242 high structural strength adhesive, *a room temperature cure adhesive*, was used. Specimens 0003, 0006, 0007 and 0008 accordingly did not fail at the hinge-substrate interface. Specimens 0009, 0011, 0012 and 0013 were not adhered with Epirez 8242 rather; the hinges were secured with two M5 bolts to the aluminium substrates seen in Fig. 8. This was examined as an extension to indicate the effects of an adhered-hinge compared to a bolted-hinge. As such, the mean of specimens 0003, 0006, 0007 and 0008 is 39.4 J/m^2 with

a standard deviation of 19.9 J/m^2 and standard error of 10.0 J/m^2. An expected value for fracture toughness of epoxy is stated between 50-1564 J/m^2 (Cambridge University Engineering Department 2003); which doesn't however specify type of epoxy and whether toughneing phases are included.

The fracture toughness determined for 2.5% specimens range from 12.3 J/m^2 to 69.6 J/m^2. Disregarding specimens 2503, 2505 and 2506 due to adhesive failure from the precracking method, the mean fracture toughness for specimens 2501, 2502 and 2504 is hence 48.5 J/m^2 with a standard deviation of 19.0 J/m^2 and a standard error of 11.0 J/m^2.

The fracture toughness determined for 5.0% specimens range from 11.1 J/m^2 to 114.7 J/m^2. Specimens 5003 and 5004 were not used to calculate the 5.0% specimen fracture toughness due to adhesive failure from precracking. The mean fracture toughness for specimens 5001, 5002, 5005, 5006, 5007 and 5008 is hence 63.8 J/m^2 with a standard deviation of 25.9 J/m^2 and a standard error of 13.0 J/m^2.

The 10% volume fraction nano-block epoxy resulted in fracture toughness values from 184.5 J/m^2 to 622.6 J/m^2. The mean fracture toughness is 339.4 J/m^2, standard deviation of 187.0 J/m^2 and standard error of 86.6 J/m^2. Initial 10% volume fraction testing, specimens 1003, 1004 and 1005, resulted in failure of the hinge-substrate interface, even with Epirez 8242 as the adherend. This signaled that the load required to propagate the crack within a 10% nano-block specimen was far greater than the load that the bond strength between hinge and substrate could withstand; the interface was the weakest element of the specimen and source of failure. Outlined by ASTM D 5528 were alternate surface preparation methods to improve hinge-substrate bond strength, however failure occurred yet again after further preparation An alternative proposal to pulling apart aluminium substrates was conducted by securing the hinge to the aluminium surface with two M5 bolts, seen in Fig. 8.

Experimental setup and analysis was conducted in the same manner with bolted hinges. The resulting force, P, versus displacement, δ, curves are shown in Fig. 13. Evident in specimens 1003 and 1004 at P = 170 N and a displacement of approximately 1 to 1.5 mm, is a variation in what should be linear loading until point of crack initiation. For both specimens, the hinges were not debonded prior to being bolted to the substrates. Conversely, specimen 1005 was completely debonded; the Epirez 8242 interface was removed. The steady load of approximately 170 N for specimen 1003 indicates failure of the existing adherend between the hinge and substrate. Similarly, specimen 1004 indicates a drop in load at 170 N of the same phenomenon until further maximum load of approximately 195 N, then presents a typical load-displacement for crack propagation. Audible failure of the hinge was observed at 170 N for both specimens 1003 and 1004. Specimens 1006 and 1007 were loaded solely by hinge, no adherend between hinge and aluminum.

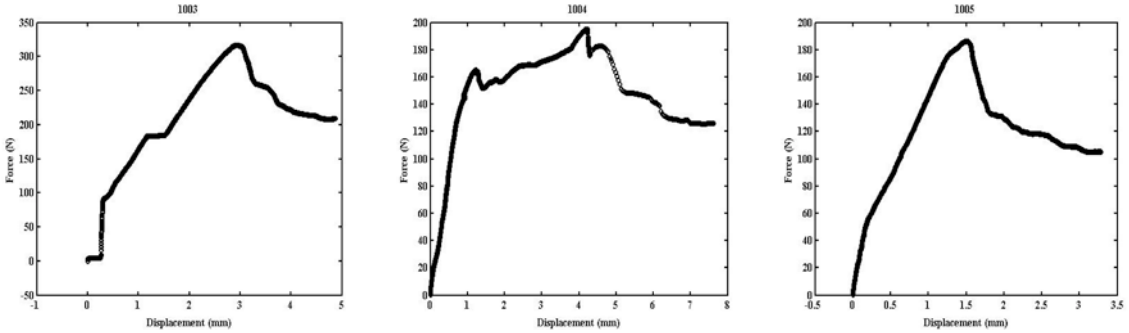

Figure 13. Load-displacement plots of specimens 1003, 1004, and 1005

By examining Fig. 14, further information as to whether an improvement to fracture toughness through the addition of nano-block copolymers can be deduced. A trend exists between 0%, 2.5% and 5.0% specimens for increasing fracture toughness. However, there is less confidence between these three ratios as to whether an improvement exists by observing the effects of the error bars. When the error bar of one mean value overlaps with another, the confidence that a difference exists between the two ratios is low. Increasing the number of samples tested can reduce the standard error and hence improve confidence. Observing the range for the 0% specimens indicates fracture toughness between 29.5 to 49.4 J/m^2, 37.5 to 59.5 J/m^2 for 2.5% and 50.9 to 76.8 J/m^2 for 5.0%. Over the interval for both 0 to 2.5% and 2.5 to 5.0%, it cannot be confidently said an improvement exists. However, between 0% and 5%, it can be conjectured that improvement to the fracture toughness exists. Given Young's modulus of 3.17 GPa for a West System® 105/206 mixture (West System® 2014), a stress intensity factor, K_{Ic}, of 0.35 MPa.m$^{0.5}$ for plane stress conditions using Eq. (13) is determined for neat epoxy. Assuming modulus remains constant with the addition of the nanophase, the resulting K_{Ic} is 1.04 MPa.m$^{0.5}$ for a 10% nano-block epoxy sample by DCB testing.

$$K^2_{IC} = GE \tag{13}$$

The consequences of loading specimens with adhered hinges to bolted hinges is indicated by the relatively higher fracture toughness of the 10% specimens to 0%, 2.5% and 5.0% Nanostrength® epoxy specimens. As the aluminium substrates separate during testing, crack propagation may additionally form sites within the hinge-substrate interface of the Epirez 8242 adherend. Specimens with adhered-bonding of the hinge to substrate may be experiencing premature adhesive failure at this interface in addition to mid-substrate crack growth. The importance of this effect cannot be distinguished from the existing load-displacement data, as failure of the hinge-substrate interface was never evident for 0%, 2.5% and 5.0% specimens. However, comparing bolted-hinge 0% to 10% specimens provides further evidence and confidence of improved fracture toughness without accounting for non-visible crack growth of the hinge-substrate interface. Shown in Fig. 15, the corrected 0% samples with bolted hinges has a mean fracture toughness of 114.1 J/m^2 (K_{Ic} of 0.60 MPa.m$^{0.5}$), standard deviation of 9.4 J/m^2 and standard error of 4.7 J/m^2 for four specimens. The comparative improvement of stress intensity factor for the bolt-hinge specimens relative to the 10% specimens is 173%. The observed improvement to bulk Mode I fracture toughness of a 0% nano-block to 10% nano-block sample by Barsotti was 207%.

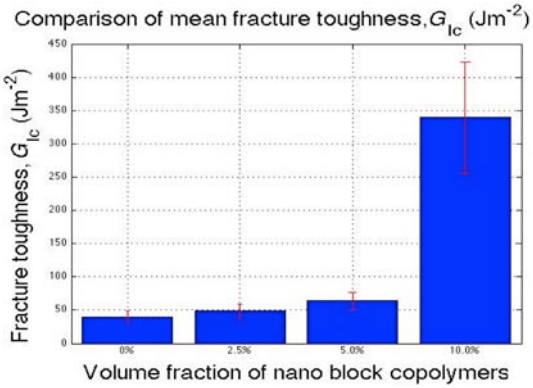

Figure 14. Comparison of mean fracture toughness, G_{Ic}

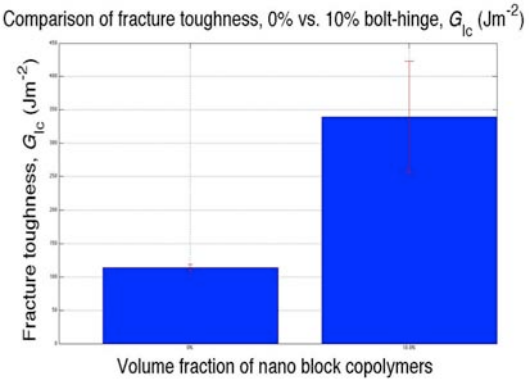

Figure 15. Comparison of 0% and 10% bolted hinge fracture toughness, G_{Ic}

V. Conclusions

The adhesive qualities of epoxy subsequently result in its primary use as a matrix constituent in composite materials. In environments requiring high resistance to crack initiation and crack growth, the application of epoxy is limited. The addition of a secondary phase can improve the fracture toughness; for this study the experimental determination of fracture toughness has been investigated for increasing levels of Nanostrength® M52N nano-block copolymers with a bisphenol A epoxy resin. Mode I fracture toughness has been determined using double cantilever beam testing. A modified simple beam theory for brittle, linear elastic behaviour, has accounted for bond line properties and non-symmetrical crack propagation of the adherend. Experimental investigation has shown improvements of stress intensity factor for Mode I failure, K_{Ic}, is 173% for 10% volume fracture nanophase.

VI. Recommendations

Mode I failure of fracture toughness has been determined by Barsotti (2008) using ASTM D 5045, SENB testing. This method differs to DCB testing whereby the material in SENB experiences plane strain conditions rather than plane stress; which in effect, influences the value of G_{Ic}.

Mode II failure of a specimen can be investigated for thin-film adherends by the end notched flexure (ENF) methodology, outlined in ASTM WK22949. Although not the primary mode of failure, Mode II still holds significance in confirming that the addition of nano-block copolymers for ENF specimens provides comparative improvement to crack initiation and growth. The preparation of specimens for ENF testing eliminates the requirement of bonding or bolting hinges to the substrates.

Acknowledgements

I would like to acknowledge and thank my supervisor Dr. Krishnakumar Shankar and Karthik Ram Ramakrishna for their ongoing support, mentoring, feedback and guidance throughout this project. A further acknowledgement is to the staff of SEIT, more specifically the workshop staff and lab technicians. Lastly, to my colleagues for experiencing this journey with me, friends, and to my family, who I am forever grateful to have in my life.

References

Abou-Hamda, MM, Megahed, MM, Hommouda, MM 1998, 'Fatigue crack growth in double cantilever beam specimen with an adhesive layer', *Engineering Fracture Mechanics*, vol. 60, pp. 605-614.

ASTM International 2007, *Standard Test Method for Mode I Interlaminar Fracture Toughness of Unidirectional Fiber-Reinforced Polymer Matrix Composites*, D 5528-01, Pennsylvania, USA.

Bagheri, R, Marouf, BT, Pearson, RA 2009, 'Rubber-Toughened Epoxies: A Critical Review', *Polymer Reviews*, vol. 49, pp. 201-225.

Barsotti, R 2008, *Nanostrength® Block Copolymers for Epoxy Toughening*, Arkema Inc., Pennsylvania, USA.

Bates, FS & Frederickson, GH 1999, 'Block Copolymers-Designer Soft Materials', *Physic Today*, vol. 52, pp. 32-38.

Blackman, B, Dear, JP, Kinloch, AJ, Osiyemi, S 1991, 'The calculation of adhesive fracture energies from double-cantilever beam test specimens', *Journal of Materials Science Letters*, vol. 10, pp. 253-256.

British Standard 2001, *Determination of the mode I adhesive fracture energy G_{IC} of structure adhesives using the double cantilever beam (DCB) and tapered double cantilever beam (TDCB) specimens*, BS 7997:2001, British Standard Institution, Bristol.

Broberg, KB 1999, *Cracks and Fracture*, Academic Press, San Diego.

Brunner, AJ, Blackman, BRK, Davies, P 2001, 'Mode I Delamination', in Moore, DR, Pavan, A, Williams, JG {ed.}, *Fracture Mechanics Testing Methods for Polymers Adhesives and Composites*, ESIS Publication 28, ed. 1, Elsevier Science Ltd, pp. 277-289.

Cambridge University Engineering Department 2003, *Materials Data Book*, Cambridge University, Cambridge.

Dalsteel Metals Pty Limited 2014, *Aluminium Alloy // Commercial Alloy – 6060*, Data Sheets, Australia, viewed 28 April 2014, <http://www.dalsteel.com.au/technical-information/datasheets/Aluminium-Alloy-6060-T5--Extrusions_144.asmx>.

Epirez 2011, *8242 Episet Structural Adhesive Gun Grade*, ITW Polymers & Fluids, New Zealand, viewed 29 April 2014, <http://www.itwpf.com.au/epirez/product.aspx?productid=75>.

Hashemi, S, Kinloch, AJ, Williams, JG 1990, 'The Analysis of Interlaminar Fracture in Uniaxial Fibre-Polymer Composites', *Proceedings of the Royal Society of London. Series A, Mathematical and Physical Sciences*, vol. 427, no. 1872, pp. 173-199.

Hossein, Y, Morteza, E, Hamed, VT, Mafi, ER 2013, 'Toughening mechanisms of rubber modified thin film epoxy resins', *Progress in Organic Coatings*, vol. 76, pp. 286-292.

Hsieh, TH, Kinloch, AJ, Masania, K, Taylor, AC, Sprenger, S 2010, 'The mechanisms and mechanics of the toughening of epoxy polymers modified with silica nanoparticles', *Polymer*, vol. 51, pp. 6284-6294.

Irwin, GR, Kies, JA 1954, 'Critical energy rate analysis of fracture strength of large welded structures', *The Welding Journal*, Res. Suppl, vol. 33, p. 193.

Jumel, J, Budzik, MK, Salem, NB, Shanahan, ME 2013, 'Instrumented End Notched Flexure – Crack propagation and process zone monitoring. Part I: Modeling and analysis', *International Journal of Solids and Structures*, vol. 50, pp. 297-309.

Khurana, P, Aggarwal, S, Narula, AK, Choudhary, V 2003, 'Studies on the curing and thermal behaviour of DGEBA in the presence of bis(4-carboxyphenyl) dimethyl silane', *Polymer International*, vol. 52, issue 6, pp. 908-917.

Kinloch, AJ 2003, 'Toughening epoxy adhesives to meet today's challenges', *MRS Bulletin*, June, pp. 455-458.

Kinloch, AJ, Johnsen, BB, Mohammad, RD, Taylor, AC, Sprenger, S 2007, 'Toughening mechanisms in novel nano-silica epoxy polymers', *Fifth Australasian Congress on Applied Mechanics 2007*, Imperial College London, London, pp. 441-446.

Kishi, H, Kunimitsu, Y, Imade, J, Oshita, S, Morishita, Y, Asada, M 2011, 'Nano-phase structures and mechanical properties of epoxy/acryl triblock copolymer alloys', *Polymer*, vol. 52, pp. 760-768.

Lamut, M, Turk, R, Torkar, M 2008, 'Determination of the adhesive fracture energy G_c of structural adhesives using DCB and Peel tests', *Materials and Geoenvironment*, vol. 55, pp. 476-489.

Le Baut, N 2005, 'Physical and Adhesive Properties of Some Materials Made by "Click" Chemistry', Honours Master of Engineering by Research thesis, University of Wollongong, Wollongong.

Morozov, E 2013, *Polymers and Composites in Engineering Chapter 4: Polymers in Engineering*, PowerPoint slides, University of New South Wales Canberra, Canberra.

Mostovoy, S & Ripling, EJ 1966, 'Fracture Toughness of an Epoxy System', *Journal of Applied Polymer Science*, vol. 10, pp. 1351-1371.

Nicu, L & Bergaud, C 1999, 'Experimental and theoretical investigations on nonlinear resonances of composite buckled microbridges', *Journal of Applied Physics*, vol. 86, pp. 5835-5840.

Pagano, NJ & Schoeppner, GA 2000, 'Delamination of Polymer Matrix Composites: Problems and Assessment', in Kelly A & Zweben CH {ed.}, *Comprehensive Composite Materials*, vol. 2, Elsevier, pp. 24-41.

Salem, NB, Budzik, MK, Jumel, J, Shanahan, MER, Lavelle, F 2013, 'Investigation of the crack front process zone in the Double Cantilever Beam test with backface strain monitoring technique', *Engineering Fracture Mechanics*, vol. 98, pp. 272-283.

Sela, N & Ishai, O 1989, 'Interlaminar fracture toughness and toughening of laminated composite materials: a review', *Composites*, vol. 20, pp. 423-435.

Shukla, A 2005, *Practical Fracture Mechanics in Design*, Marcel Dekker, Rhode Island, USA.

West System® 2014, *Typical Physical Properties*, West System Inc., viewed 18 May 2014, <www.westsystem.com/ss/typical-physical-properties/>

Wetzel, B, Rosso, P, Hauper, F, Friedrich, K 2006, 'Epoxy nanocomposites – fracture and toughening mechanisms', *Engineering Fracture Mechanics*, vol. 73, pp. 2375-2398.

Yahyaie, H, Ebrahimi, M, Tahami, HV, Mafi, ER 2013, 'Toughening mechanisms of rubber modified thin film epoxy resins', *Progress in Organic Coatings*, vol. 76, pp. 286-292.

Yang, J 1998, 'Part II: Modifications of epoxy resins with functional hyperbranched poly (arylene ester)s', PhD thesis, Virginia State University, Blacksburg.

Zamanian, M, Mortezaei, M, Salehnia, B, Jam, JE 2013, 'Fracture toughness of epoxy polymer modified with nanosilica particles: Particle size effect', *Engineering Fracture Mechanics*, vol. 97, pp. 193-206.

Zhao, Q & Hoa, SV 2007, 'Toughening Mechanism of Epoxy Resins with Micro/Nano Particles', *Journal of Composite Materials*, vol. 41, pp. 201-218.